DOI: 10.19884/j.1672-5220.202304010

Numerical Simulation of Flow Field and Flow State Division in Thin-Film Evaporators

CHEN Xing, PENG Yitian*, HUANG Yao, ZOU Kun
College of Mechanical Engineering, Donghua University, Shanghai 201620, China

Abstract: The flow field and flow state of thin-film evaporators are complex, and it is significant to effectively divide and quantify the flow field and flow state, as well as to study the internal flow field distribution and material mixing characteristics to improve the efficiency of thin-film evaporators. By using computational fluid dynamics (CFD) numerical simulation, the distribution pattern of the high-viscosity fluid flow field in the thin-film evaporators was obtained. It was found that the staggered interrupted blades could greatly promote material mixing and transportation, and impact the film formation of high-viscosity materials on the evaporator wall. Furthermore, a flow field state recognition method based on radial volume fraction statistics was proposed, and could quantitatively describe the internal flow field of thin-film evaporators. The method divides the high-viscosity materials in the thin-film evaporators into three flow states, the liquid film state, the exchange state and the liquid mass state. The three states of materials could be quantitatively described. The results show that the materials in the exchange state can connect the liquid film and the liquid mass, complete the material mixing and exchange, renew the liquid film, and maintain continuous and efficient liquid film evaporation.

Key words: flow state division; material mixing; thin-film evaporator; numerical simulation
CLC number: TS152; TH6 **Document code**: A
Article ID: 1672-5220(2024)05-0525-11

Open Science Identity (OSID)

0 Introduction

A thin-film evaporator through the rotation of the blade will be forced to scrape the fluid material into a uniform thickness of the liquid film so that materials can obtain high heat and mass transfer efficiency and realize rapid evaporation and concentration, which plays an important role in medicine, chemistry, textiles, food and other fields[1-3]. Among them, fluid flow, film-forming states, distribution characteristics of the flow field, and the mixed transmission mechanism of the flow field in thin-film evaporators have decisive influences on continuous and efficient fluid evaporation in the evaporators. Researchers have carried out a lot of research on fluid flow and heat transfer characteristics in thin-film evaporators[4], and they found that flow field distribution had an important effect on heat and mass transfer in the evaporators, and played a key role in the rapid evaporation of fluid in the evaporators.

There are two main movements of the fluid in the traditional straight-plate vane thin-film evaporators. The first movement is the spiral vertical descent of the circular wave, and the cylindrical circular wave material group moves along with the direction of blade rotation. The other movement is a scraping film gap between the blade tip and the wall, and the material flows down at the gap and near the wall. Komori et al.[5] studied the mixing mechanism of the flow state in the thin-film evaporators and proposed to improve the structure of the evaporators by replacing the traditional single-row blade with a multi-row blade[6-7]. It was found that a multi-row blade could effectively promote material exchange between the circular wave and the film. In addition, the influence of the arrangement spacing and inclination angle of the multiple rows of blades on the evaporator flow field was also investigated. Mckelvey et al.[8] believed that the flow mixing of circular waves was the key to the efficient operation of the whole thin-film evaporators. Although it is difficult for fluids with high viscosity to carry out effective flow mixing by gravity, to carry out the rapid evaporation of materials, material exchange and renewal can be realized between the circular wave and the liquid film so that the liquid film can continue to evaporate with high quality. These flow structures indicate that fluid flow and mixed transport have an important effect on heat transfer between materials, enabling more efficient evaporation.

In the early stages, the numerical simulation of the flow field in the thin-film evaporators was a two-dimensional (2D) simulation study, lacking the axial transmission characteristics of fluids. Therefore, the

Received date: 2023-04-18
Foundation items: National Natural Science Foundation of China (Nos. 51905089 and 52075093); Special Fund for Basic Research and Operating Costs of Central Colleges and Universities, China (No. 22320D-31); Open Fund for National Key Laboratory of Tribology of Tsinghua University, China (No. SKLTKF20B05)
* Correspondence should be addressed to PENG Yitian, email: yitianpeng@dhu.edu.cn
Citation: CHEN X, PENG Y T, HUANG Y, et al. Numerical simulation of flow field and flow state division in thin-film evaporators[J]. *Journal of Donghua University (English Edition)*, 2024, 41(5): 525-535.

numerical simulation of the evaporators gradually changed from a 2D cross-section model[9] to a three-dimensional (3D) model[10-12], and more exploration was carried out on the axial transmission of the evaporator flow field and material mixing. The 3D two-phase flow field model proposed by Pawar et al.[10] took into account the influence of gas-liquid two-phase flow and axial material transfer. The simulation results showed that the material flows in the gap between the blade tip and its wall surface, indicating that the gap played an extremely important role. Wang et al.[11] studied the fluid flow in the evaporators to optimize the structure of the evaporators. He et al.[12] established a circular wave axial flow model to study the changes in the axial velocity by adjusting blade speed, feed amount, material viscosity and other conditions. Through the study and analysis of images, Guo et al.[13] found that four different forms of the liquid film appeared on the wall of the evaporators during the whole working process. Researchers have studied the evaporator blades and the residence time of the material in the evaporators. Three different hydrodynamic states of the material were found to arise in the thin-film evaporators[14], and the formation conditions and effects of these flow states were discussed. Through the study of the 3D evaporator model, it is found that there are a variety of different flow forms in the evaporator flow field. Through the analysis of the convection state, it is possible to explore the distribution state of the evaporator flow field and the characteristics of the material mixed transport.

The improvement of the production capacity of thin-film evaporators is an urgent problem to be solved, and the quality of the flow field in thin-film evaporators has a significant impact on their production capacity. The above studies are based on Newtonian fluids with relatively low viscosity. The common materials processed in the evaporators during production, such as food, fiber and resin, are mostly high-viscosity non-Newtonian fluids, and their film-forming mechanism and states in the evaporators will be more complex. Zheng et al.[15] calculated the flow field distribution of non-Newtonian fluids with different viscosities in thin-film evaporators and believed that with the gradual increase of the viscosities, the film formation of the thin-film evaporator walls became worse. Therefore, it is proposed to interrupt and cross-combine the straight blades to increase the mixing and spreading of materials by the blades, and the multiple rows of staggered blades can promote the material exchange of the circular wave and the liquid film, increase the axial transmission of materials[16], improve the distribution of the evaporator flow field, and enhance the production efficiency.

Drawing on the above experience, this paper adopts the computational fluid dynamics (CFD) method[17] to conduct a 3D two-phase flow simulation[18]. The simulation focuses on the complex flow field of the film evaporators with multiple rows of staggered blades under the high-viscosity non-Newtonian fluid material[5-6,15]. Furthermore, the study examines the flow and distribution states of the internal flow field of the film evaporators. A new flow field state identification method based on radial volume fraction statistics is proposed to classify the material flow state, and through flow state analysis, the evaporator flow field distribution states and material mixed transmission characteristics are explored, and the flow inside the evaporators is described more accurately to achieve a quantitative description and evaluation of the flow field distribution state.

1 Physical Mathematical Model

1.1 Model establishment

The CFD software Fluent was used for the numerical simulation. Figure 1(a) shows the staggered interrupted blade structure of the evaporators. There are 18 rows of blades uniformly distributed on the rotor, and the blades are composed of two different types alternately distributed to complete the spreading and transmission of the evaporator materials. Figure 1(b) is a schematic diagram of the fluid domain of numerical calculation. The evaporator model is referred to as the Komori experimental model. The model is composed of a wall surface, a rotor, a rotating blade, an outlet and an inlet. In this model, the wall diameter of the evaporator is 250 mm, the thickness of the blade is 3 mm, the length is 150 mm, and the distance between the tip of the blade on the rotor and the wall of the evaporator is 1 mm.

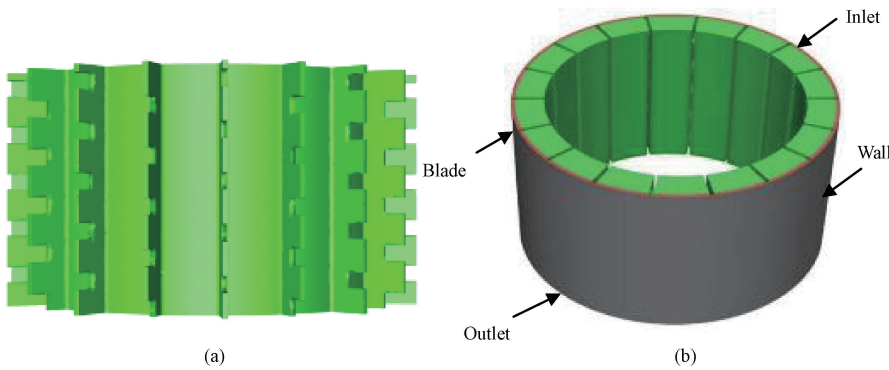

Fig. 1 Model structure: (a) staggered interrupted blade structure; (b) calculation geometric model

The pressure solver was used to solve the simulation calculation, and the pressure-velocity coupling algorithm was used. The fluid of the whole simulation calculation is assumed to be incompressible fluid, and only the calculation under the condition of no heat transfer in the evaporator is considered. For incompressible fluid motion without heat transfer, the momentum equation and the continuity equation[15] are:

$$\frac{\partial}{\partial t}(\rho \boldsymbol{U}) + \nabla \cdot (\rho \boldsymbol{U}\boldsymbol{U}) = -\nabla p + \nabla \cdot \left[\mu(\nabla \boldsymbol{U} + (\nabla \boldsymbol{U})^{\mathrm{T}}) - \frac{2}{3}\rho k \boldsymbol{I}\right] - \rho(\boldsymbol{\Omega}\boldsymbol{U}) + \rho g, \quad (1)$$

$$\nabla \cdot \boldsymbol{U} = 0, \quad (2)$$

where $\boldsymbol{U}$ is fluid velocity vector; μ is fluid viscosity; p is fluid pressure; ρ is density; k is turbulent kinetic energy; $\boldsymbol{\Omega}$ is blade rotation angular velocity vector; $\boldsymbol{I}$ is identity tensor; g is the gravitational acceleration.

There are two kinds of media in the working state of the thin-film evaporators: liquid material requiring rapid evaporation and air existing in the evaporators. Therefore, to simulate and calculate the gas-liquid two-phase internal flow field state and mixing of the evaporator more accurately, this paper adopts the volume of fluid (VOF) method[19-20] to describe the gas-liquid interface. According to the computational storage method of the VOF model, the following physical characteristics in its control volume are

$$\rho = \rho_1 \alpha + (1 - \alpha)\rho_g, \quad (3)$$

$$\mu = \mu_1 \alpha + (1 - \alpha)\mu_g, \quad (4)$$

where ρ_1 is the liquid phase density; ρ_g is the gas phase density; μ_1 is the liquid phase viscosity; μ_g is the gas phase viscosity; α is the liquid phase volume fraction.

In thin-film evaporators with complex internal flow patterns, due to the forced film forming of the blade, the material near the wall presents a complex turbulent state. In this paper, according to the actual situation of the evaporators, the shear stress transport (SST) k-ω turbulence model[21-22] is used to calculate the turbulence model.

For turbulent kinetic energy,

$$\frac{\partial(\rho k)}{\partial t} + \nabla \cdot (\rho k u) = \nabla \cdot \left((\mu + \frac{\mu_t}{\sigma_k})\nabla \cdot k\right) + G_k - Y_k, \quad (5)$$

for specific dissipation rate,

$$\frac{\partial(\rho \omega)}{\partial t} + \nabla \cdot (\rho \omega u) = \nabla \cdot \left(\left(\mu + \frac{\mu_t}{\sigma_\omega}\right)\nabla \cdot \omega\right) + G_\omega - Y_k + D_\omega, \quad (6)$$

where G_k is the generation of k; G_ω is the generation of ω; Y_k is the dissipation of k; Y_ω is the dissipation of ω; σ_k is the surface tension coefficient of k; σ_ω is the surface tension coefficient of ω; μ_t is the turbulent viscosity; D_ω is the cross-diffusion term.

The evaporator inlet condition is set for the inlet mass flow rate, and the mass flow rate value is 0.1 kg/s. The outlet condition is set as the pressure outlet, connected with the external environment, and the pressure value is set as the standard atmospheric pressure. A single-motion reference frame model is used to realize the uniform rotation of the rotor and the blade in the evaporator. The internal fluid calculation domain of the evaporator rotates at a speed of 90 r/min. The velocity of the rotor and the blade relative to the fluid domain is zero, and the wall surface is stationary. The second-order upwind algorithm is used to solve the momentum equation, and the rest are left with default settings. When the setting is completed, and the calculation is initialized, the inside of the evaporator is set to be filled with gas to conform to the real production environment.

1.2 Analog medium

In the thin-film evaporators for processing high-viscosity non-Newtonian fluids, the viscosity of the non-Newtonian fluid μ and shear strain rate S are not up to the linear function relation. Therefore, the physical properties of non-Newtonian fluids are more complex, and their rheological mathematical models are generally invoked to describe their rheological properties. The material under study is a food processing material, fenugreek gum solution[23], and the rheological model of this material conforms to the Carreau model function relation:

$$\mu = \mu_\infty + (\mu_0 - \mu_\infty)\left[1 + (\Gamma S)^2\right]^{\frac{n-1}{2}}, \quad (7)$$

where Γ is relaxation time; n is the non-Newtonian index; μ_0 is the zero shear viscosity; μ_∞ is the limited shear viscosity. In this research, Γ is 10.149 s; n is 0.413 3; μ_0 is 38.803 Pa·s; μ_∞ is 0.009 978 2 Pa·s.

2 Results and Discussion

2.1 Flow field distribution

Figure 2 shows the flow field distribution of fenugreek gum solution in an 18-row interrupted blade thin-film evaporator with a mass flow rate of 0.1 kg/s from the inlet at a speed of 90 r/min. Figures 2(a) and 2(b) show the internal flow field distribution diagram of the evaporator from different perspectives, respectively. The annular liquid film spreading on the outer wall and the liquid mass at the blade tip can be seen in Fig. 2(a), which can also be observed from the flow field distribution diagram inside the evaporator. The wall of the evaporator has a layer of the uniform liquid film, which is the key to the evaporation and dehydration of the thin-film evaporator. However, in the inner part of the liquid film region, different from the circular wave column liquid mass formed by the straight scraper blade

in traditional research, the evaporator forms a periodic distribution of inverted "L" shaped strip liquid mass. The tip of the evaporator blade is enlarged, as shown in Fig. 2(c). In Fig. 2(c), it can be seen that there are circular liquid masses on the leading edge of the blade and irregular material protrusions at the trailing edge of the blade. The strip liquid mass in the blue circle in Fig. 2(b) is enlarged, as shown in Fig. 2(d). This strip liquid mass can be divided into two parts according to the two sides of the "L" shape, and the two parts are located on both sides of the blade (the hollowed-out region along the axial direction of the liquid film is the position of the blade). The part of the "L" shaped strip liquid mass locates at the leading edge of the blade, as shown on the right side of the blade, is the liquid mass scraped out of the blade. It can be seen that its shape is similar to the liquid mass with the shape of a circular wave. The part of the "L" shaped strip liquid mass located at the trailing edge of the blade is called the liquid strand, which extends in a slightly downward horizontal direction, as shown on the left side of the blade. The material masses accumulate in the leading edge of the blade flow out at the blade gap and form a trailing tail at the trailing edge of the blade during the blade rotating scraping film process. This tail accumulates at the leading edge of the next blade. The "L" shaped material distribution formed by such liquid mass and liquid strand realizes the efficient material exchange between the films of high-viscosity non-Newtonian materials in the evaporator, as well as the effective material transmission along the axial direction, so that the materials can be better spread on the wall. It solves the problem that such high-viscosity non-Newtonian fluid materials are not easy to form films on the evaporator wall.

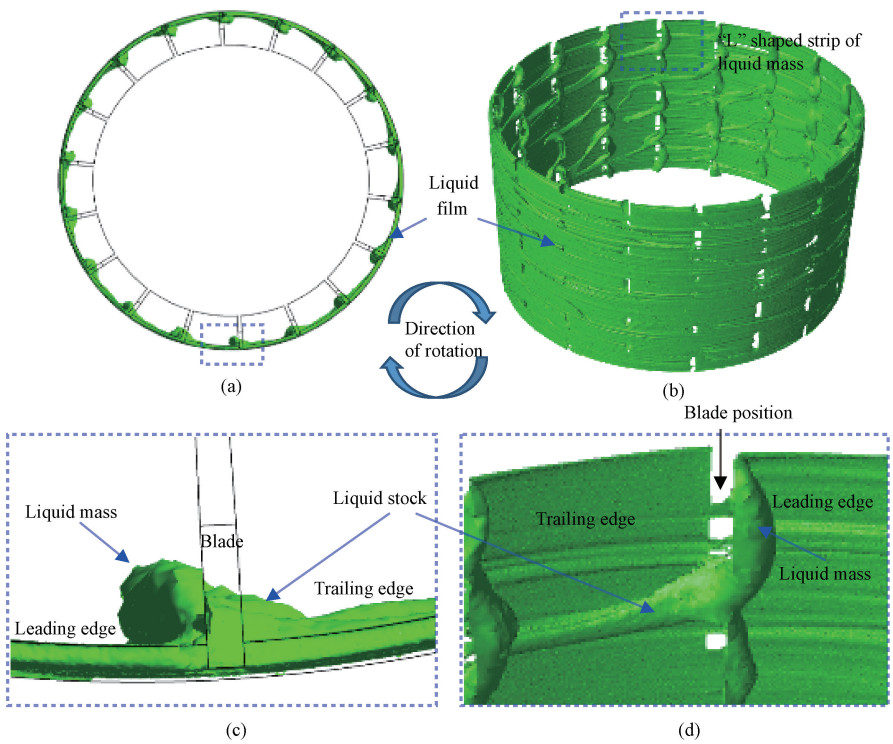

Fig. 2 Flow field distribution results: (a) top view of flow field distribution; (b) oblique view of flow field distribution; (c) enlarged view of flow field at blade position; (d) enlarged view of "L" shaped strip liquid mass

However, although such a blade structure is more beneficial to the film formation of high-viscosity non-Newtonian fluid materials than the traditional form, its flow field state is too complex. Figure 3 shows the flow field distribution of different sections. The red with the value of 1.0 represents the liquid phase, while the blue with the value of 0 represents the gas phase. Figure 3(a) shows the cloud image of the radial section of the flow field. The liquid mass at the leading edge of the blade and the liquid strands at the trailing edge of the blade can be observed by enlarging the flow field near the two blades. The shape of the liquid mass is regular and round, while the shape of the liquid strand is an uneven strip. It can be concluded that the distribution of materials in the radial section of this flow field is very different from that of the traditional circular wave-feeding film (Fig. 4).

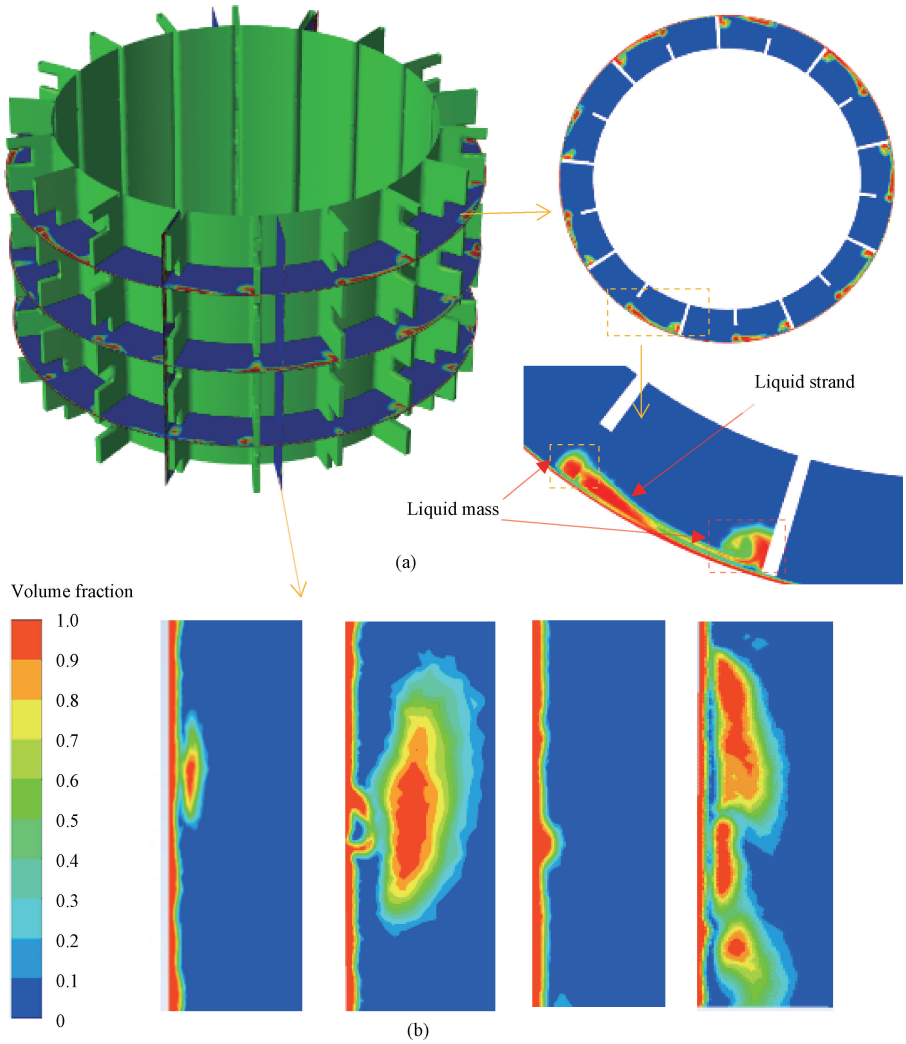

Fig. 3 Comparison of flow fields in different sections: (a) cross-section cloud view of radial flow field; (b) cross-section cloud view of axial flow field

In addition, the cross-section cloud diagram of the axial flow field of gas-liquid integration number obtained from different positions inside the evaporator (as shown in Fig. 3(b)) can also be derived. Due to the presence of "L" shaped strip liquid mass formed by the action of staggered interrupting blades, the axial flow field inside the evaporator is more complex than that of the traditional straight blades[15]. Figure 4 (a) is a schematic diagram of fluid flow in the traditional thin film evaporator, which is mainly composed of circular waves and liquid films, and the fluid distribution is relatively simple in axial and circumferential directions. Figure 4 (b) shows the flow field distribution under different viscosities. With the increase in viscosity, the film-forming integrity deteriorates. The group and the film of the flow field in the traditional straight-blade evaporator only exist at the position where the circular wave and liquid film contact, and the interaction interface is relatively regular. There is no interaction between the liquid films at other positions, that is, the ability to renew liquid film is limited. However, the evaporator in this paper adopts staggered interrupted blades, so that the internal flow field has a periodic distribution of "L" shaped strip liquid mass in addition to the liquid film, which greatly increases the interaction probability between the liquid film and the liquid mass. At the same time, it can be seen from the axial section that the interaction form of the films is more complex, and the interaction between the films will change the state of the liquid film itself. Due to the complexity of the distribution form of the overall flow field, it is difficult to accurately divide and quantitatively analyze the liquid film and liquid mass regions, as well as to describe the interaction between the films.

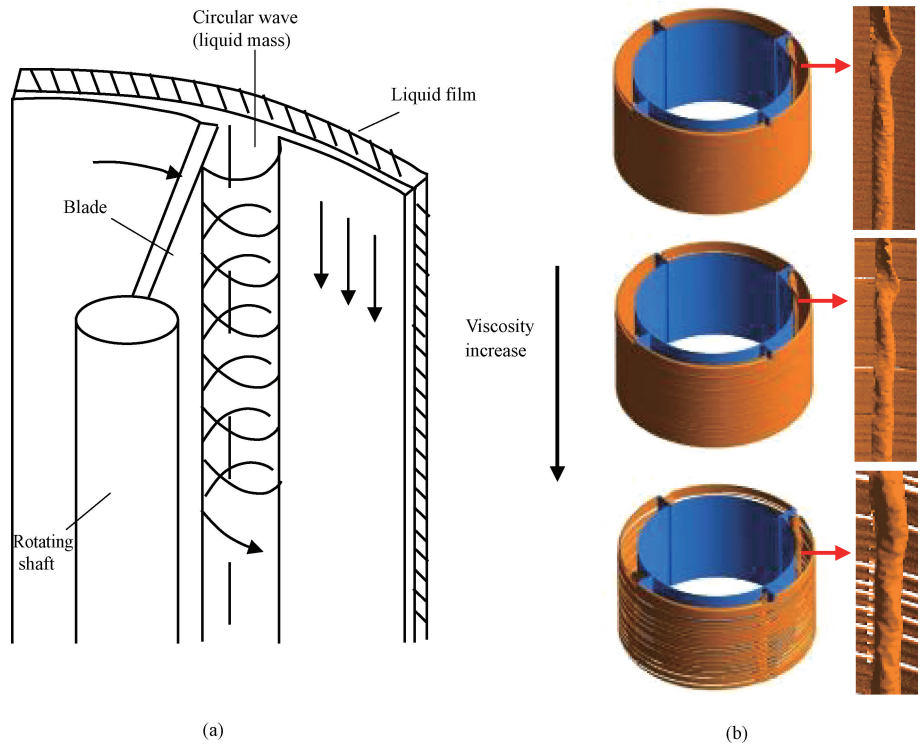

Fig. 4 Flow field distribution of traditional thin-film evaporator: (a) schematic diagram of fluid flow[4]; (b) flow field distribution of material with different viscosities[15]

2.2 Flow division and flow action mechanism

Because of the great difference in the evaporator flow field state in different positions, a single section is difficult to reflect the whole property of the flow field. Therefore, the volume fraction of all grid nodes in the whole model is extracted and analyzed statistically to solve the above problems. For the real flow field inside the evaporator, materials mainly exist in two forms, one is the liquid film, and the other is the liquid mass ("L" shaped strip liquid mass contains liquid mass at the leading edge of the blade and liquid strand at the trailing edge of the blade), and the two need to constantly interact for material and heat exchange. Both of these two forms of materials have a gas-liquid interface. When they contact for material exchange, the gas-liquid interface of the liquid mass and the liquid film also interact (as shown in Fig. 5(a)). Therefore, the quantity distribution of the gas-liquid interface reaches a peak in the interaction zone between the mass and the film. Firstly, the data of grid nodes with a volume fraction of 0.5 is extracted and analyzed. The gas-liquid material with a volume fraction of 0.5 is between the pure gas phase and the pure liquid phase, and such nodes represent the gas-liquid interface of the material. The location of the material interface is determined by the number of peak values of 0.5 volume fraction grid nodes, and then the mean value and the standard deviation of the radial volume fraction are calculated.

As can be seen from Fig. 5(b), the region with the highest concentration of the gas-liquid interface is 0.6–1.1 mm, that is, the location where a large amount of substance exchange occurs between liquid masses and liquid films. We made statistics on the distribution of the gas-liquid interface at different radial distances for the material volume fraction of 0.5, analyzed and counted the interface positions of liquid masses and liquid films between materials and the interface positions of materials and gases, and then judged the mixing exchange between materials and the exchange region between materials and gas. As shown in Fig. 5(b), the gas-liquid material with a 0.5 volume fraction is less distributed at the radial distances of 0–0.6 mm and 1.1 mm, and more distributed at the radial distances of 0.6–1.1 mm. According to the cross-section cloud diagram of the axial flow field in Fig. 5(a), it can be concluded that the region between 0.6 mm and 1.1 mm is the region with more dots at the gas-liquid interface of liquid films and liquid masses, which is a film exchange region for material renewal between related materials.

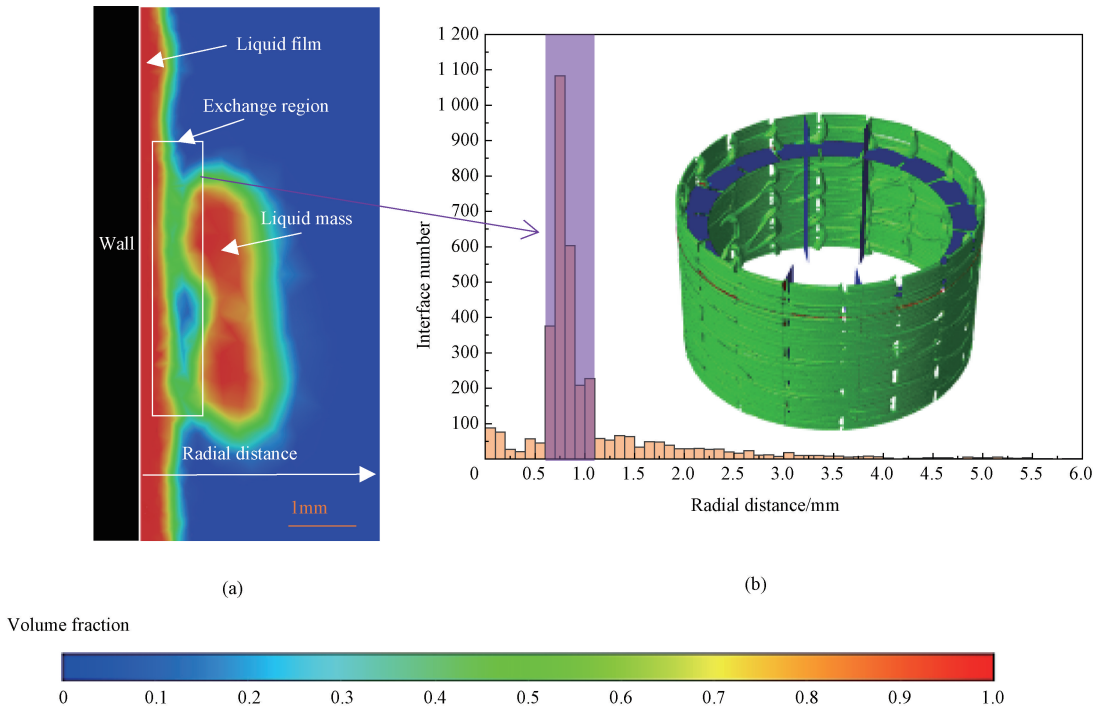

Fig. 5 Gas-liquid interface judgment: (a) cross-section cloud view of axial flow field; (b) distribution histogram of different radial distances of materials at the gas-liquid interface with volume fraction of 0.5

The identification of the exchange region can help us further understand the flow field distribution inside the evaporator. The mean volume fraction and its standard deviation of each grid node under different radial distances were further counted, and the variation curve of the volume fraction with the radial distance was drawn. Figure 6(a) is a radial volume fraction calculation diagram. Assume that the red liquid film is the pure liquid phase, with a volume fraction of 1.0, the blue is a pure gas phase, the volume fraction is 0, and the specific radial distance of the mean volume fraction v is

$$v = L_{liq}/(L_{liq} + L_{gas}), \tag{8}$$

where L_{liq} is the length of the liquid phase; L_{gas} is the length of the gas phase. The average volume fraction of the material can reflect the two-phase ratio of the liquid phase to the gas phase, reflecting the specific state properties of the material, while the standard deviation of the volume fraction of the material can reflect the exchange amplitude of the gas-liquid two-phase material mixing in this region. Generally speaking, the larger the average volume fraction, the more liquid phase composition, whereas the more gas phase composition; the larger the standard deviation of the volume fraction, the more intense the material exchange and heat exchange between liquid masses and liquid films.

Figure 6(a) shows that the mean volume fraction changes with radial distance, and the curve can be divided into three regions according to its changing trend. In the first region, that is, in the region of 0–0.6 mm radial distance, the average volume fraction of the material is stable around 1.0, indicating that the material in this region is all liquid phase, which is the liquid film region. The standard deviation line segment shows a small range and a small decline, indicating that the material state is mainly liquid, and less involved in gas-liquid two-phase mixing exchange. In the second region, the radial distance is 0.6 – 1.1 mm and is exactly consistent with the interaction region of the masses and films obtained above. It can be seen that the mean volume fraction of the material in this region drops sharply, indicating that it begins to approach the gas-liquid interface of the liquid film, and the continuous introduction of the gas phase makes the mean volume fraction decrease continuously. However, the standard deviation increases sharply, indicating that the gas-liquid phase in this region is violently mixed. It is further verified that the most concentrated region of gas-liquid with a volume fraction of 0.5 in Fig. 5 is the region where the exchange between the liquid film and the liquid mass is the most important and intense. The addition and mixing of the gas phase make the volume fraction of the liquid phase decrease continuously. Correspondingly, the standard deviation begins to increase sharply. The wider the distribution range of the material volume fraction in the exchange region, the larger the standard deviation of the volume fraction and the higher the stirring efficiency. The third region is the region beyond the radial distance of 1.1 mm. The average volume fraction of materials in the third region is low and relatively stable, indicating that the gas phase is the main part of this region. It is the liquid-mass region, where materials exist in the form of

liquid masses and are surrounded by a large amount of gas. In this region, there is less gas-liquid coexistence and less mutual doping, and the volume fraction difference is large, so the standard deviation at the two ends of the liquid-mass interface region presents a rising phenomenon. When it gets to the edge of the outermost blob, the blob gets smaller and is almost all gas, the standard deviation is going to turn around from here. This indicates that with the increase in radial distance, the gas-liquid component gradually tends to be stable, indicating that this region is mainly composed of gas-phase air.

Based on the above analyses, the flow field pattern inside the thin-film evaporator can be divided into three regions in terms of the radial distance to the wall. In the first region, the radial distance is 0–0.6 mm, the average volume fraction of the material is close to 1.0, and the standard deviation is relatively stable and small. It can be determined as the stable and uniform liquid film region. In the second region, the radial distance is 0.6–1.1 mm, the average volume fraction of the materials decreases sharply from 1.0 to about 0.1, and the standard deviation also increases sharply, indicating that the materials are mixed and stirred relatively well and that the gas-liquid phase has a two-phase staggered mixing distribution. It can be determined as the exchange region where the mixing and exchange of materials takes place. In the third region, when the radial distance is beyond 1.1 mm, the material volume fraction is relatively stable and within a low range. It can be determined as the liquid mass region.

Figure 6(b) shows the distribution of material volume fraction in the total region with a radial distance of 6 mm. The volume fraction value of the material with a high volume fraction is close to 1.0 (pure liquid phase), which is mainly concentrated in the region with a small radial distance, while the volume fraction value of the material with a low volume fraction is close to 0 (pure gas phase), which is mainly concentrated in the region with a large radial distance. According to the three regions divided above, the radial volume fraction distribution is statistically analyzed. The volume fraction distribution of materials in the liquid film region, the exchange region and the liquid mass region are shown in Figs. 6(c), 6(d) and 6(e). In the liquid film region, the material volume fraction distribution is mainly pure liquid phase. In the exchange region, the material volume fraction distribution is relatively wide, and there are different degrees of distribution. Within a small radial distance, that is, near the end of the liquid film, the distribution of the material with a large volume fraction is more obvious. Within a large radial distance, that is, near the end of the liquid mass, the distribution of the material with a small volume fraction is more obvious. In the liquid mass region, there is no more material distribution of other volume fractions, and the volume fractions of 0 and 1.0 are more distributed.

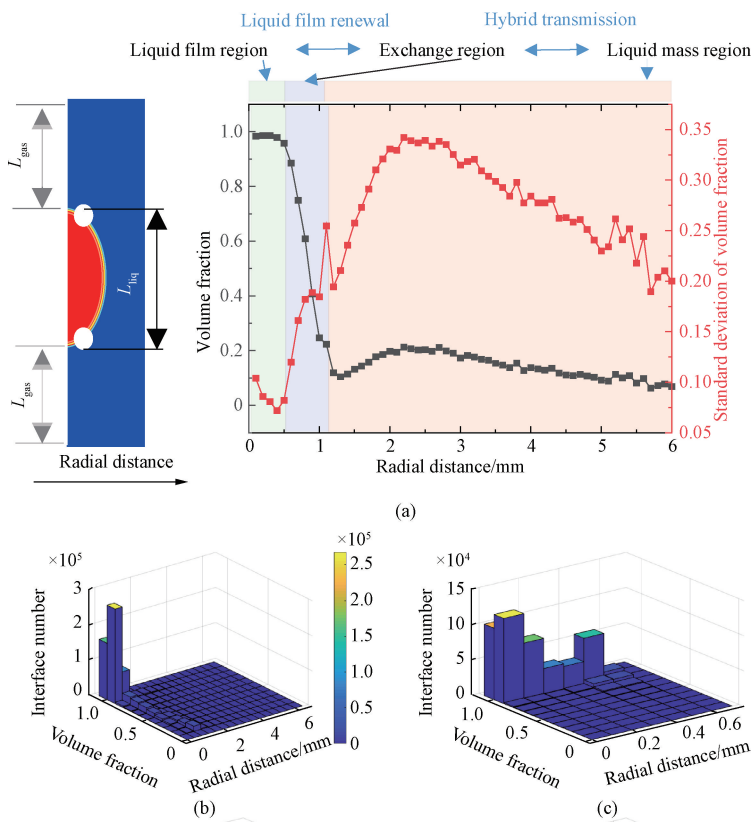

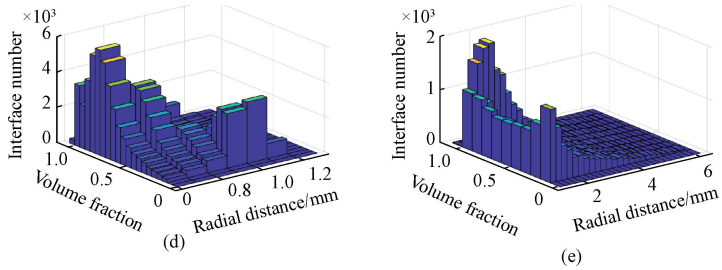

Fig. 6 Material volume fraction distribution statistics: (a) curve of volume fraction with radial distance; (b) total region volume fraction distribution; (c) liquid film region volume fraction distribution; (d) exchange region volume fraction distribution; (e) liquid mass volume fraction distribution

For the above calculation method of the volume fraction within a specific radial distance, the flow field of different liquid films in the evaporator has a different performance, which can be used to judge the shape of the liquid film. As shown in Figs. 7(a), 7(b) and 7(c), the mean volume fraction curves of the liquid films with different shapes are quite different when calculating the mean volume fraction. In Fig. 7, P_0 and P_1 represent the pure gas phase and the pure liquid phase, respectively. Therefore, the material flow state in the evaporator can be analyzed and judged based on the radial volume fraction mean curve.

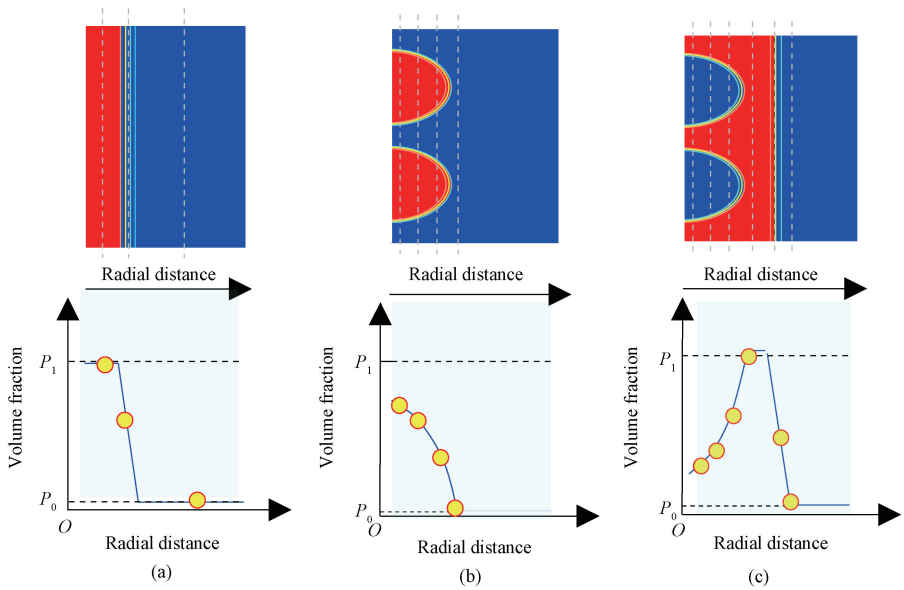

Fig. 7 Comparison of volume fraction curves of liquid films with different forms: (a) schematic diagram of calculating radial volume fraction of homogeneous liquid film; (b) schematic diagram of calculating radial volume fraction of raised liquid film; (c) schematic diagram of calculating radial volume fraction of air gap liquid film

Through the above analysis and the distribution of the gas-liquid interface along the radial distance, the flow field inside the film evaporators can be accurately divided into three states. The state of the liquid film and the specific position of the gas-liquid interface of materials can be known through the mean volume fraction of materials within different radial distances. The standard deviation of the mean volume fraction can also describe and measure the intensity of film exchange in the exchange zone. Through the flow state division, the mechanism of action between the flow states in the evaporators is understood. The interaction of the three flow states is an important support for the formation of a sustainable and efficient evaporation flow field in the evaporators.

3 Conclusions

In this paper, a computational model of high-viscosity non-Newtonian fluid in 18 rows of thin-film evaporators with staggered blades is established using CFD, and the flow field distribution characteristics of high-viscosity materials in evaporators are obtained. A flow field pattern recognition method based on radial volume fraction statistics is proposed, which can be used to classify the flow field and the state in evaporators. The

results are expressed as follows.

1) The staggered interrupted blades can make the high-viscosity non-Newtonian fluid carry out effective axial transmission, promote material exchange between materials, and solve the problem that the high-viscosity non-Newtonian material does not easily form a film on the evaporator wall.

2) The mean curves of the radial distance volume fraction of different flow fields in the evaporators are different. The flow state of the material flow field in the evaporators can be analyzed and judged using the mean curves of the radial volume fraction.

3) Materials in the evaporators can be divided into three types: materials in the liquid film region, materials in the exchange region, and materials in the liquid mass region. It is one of the most important features of thin-film evaporators that materials in the liquid film region can increase the evaporation efficiency of the thin film. The higher the average volume fraction of materials in this region, the better the quality of the liquid film. The materials in the exchange region can connect the liquid film and the liquid mass inside the evaporators to complete the material mixing exchange and renewal. The larger the standard deviation of the material volume fraction, the more intense the exchange of substances, and the more continuous and efficient the evaporation of the liquid film will be. The liquid mass region can gather materials and provide raw materials for liquid mass and liquid film material exchange.

References

[1] JASCH K, GRÜTZNER T, ROSENTHAL G, et al. Experimental investigation of the residence time behavior of a wiped film evaporator [J]. *Chemical Engineering Research and Design*, 2021, 165: 162-171.

[2] LAORETANI D S, IRIBARREN O A. Optimization of the recycle structure of multiple stages molecular distillation [J]. *Chemical Engineering Research and Design*, 2018, 130: 35-41.

[3] ZHUANG X P, LIU X F, CHENG B W, et al. Preparation and properties of antibacterial lyocell fibers containing chitosan derivative[J]. *Journal of Donghua University (English Edition)*, 2006, 23(5): 83-86.

[4] APPELHAUS D, JASCH K, JAHNKE S, et al. A new approach to simulate the fluid dynamics in a wiped film evaporator using modelica [J]. *Chemical Engineering Research and Design*, 2020, 161: 115-124.

[5] KOMORI S, TAKATA K, MURAKAMI Y. Flow structure and mixing mechanism in an agitated thin-film evaporator [J]. *Journal of Chemical Engineering of Japan*, 1988, 21(6): 639-644.

[6] KOMORI S, TAKATA K, MURAKAMI Y. Flow and mixing characteristics in an agitated thin-film evaporator with vertically aligned blades [J]. *Journal of Chemical Engineering of Japan*, 1989, 22(4): 346-351.

[7] KOMORI S, TAKATA K, NAGAOSA R, et al. The effects of multiple inclined blades on flow and mixing characteristics in an agitated thin-film evaporator[J]. *Journal of Chemical Engineering of Japan*, 1990, 23(5): 550-555.

[8] MCKELVEY J M, SHARPS G V J. Fluid transport in thin film polymer processors [J]. *Polymer Engineering & Science*, 1979, 19(9): 651-659.

[9] YATAGHENE M, PRUVOST J, FAYOLLE F, et al. CFD analysis of the flow pattern and local shear rate in a scraped surface heat exchanger [J]. *Chemical Engineering and Processing: Process Intensification*, 2008, 47(9/10): 1550-1561.

[10] PAWAR S B, MUJUMDAR A S, THORAT B N. CFD analysis of flow pattern in the agitated thin film evaporator [J]. *Chemical Engineering Research and Design*, 2012, 90(6): 757-765.

[11] WANG C, ZHANG J M, LIU B, et al. Initial liquid film distribution and feed structure optimization in wiped film molecular distillter [J]. *Chemical Engineering*, 2019, 47(7): 20-24, 46. (in Chinese)

[12] HE X H, TANG P, LI J, et al. Numerical simulation of fluid flow characteristics in thin film evaporator [J]. *Chinese Journal of Process Engineering*, 2005, 5: 357-363. (in Chinese)

[13] GUO K, YUAN M, XU S L. Study on liquid flow state in scraping film molecular distillation [J]. *Journal of Chemical Engineering of Chinese Universities*, 2009, 23: 187-192. (in Chinese)

[14] CVENGROŠ J, POLLÁK Š, MICOV M, et al. Film wiping in the molecular evaporator [J]. *Chemical Engineering Journal*, 2001, 81(1/2/3): 9-14.

[15] ZHENG S S, HUANG Y, ZOU K, et al. Numerical simulation of flow field characteristics of non-Newtonian fluid in film scraping evaporator[J]. *Acta Physica Sinica*, 2022, 71: 197-208. (in Chinese)

[16] WANG Z W, CHEN L L, HUANG Y, et al. Numerical simulation of flow field distribution and transmission characteristics in thin film evaporator [J]. *Journal of Donghua University (Natural Science)*, 2022, 48(1): 1-11. (in Chinese)

[17] WANG Y R, FU H M. 3D visual plant models in computational fluid dynamics simulation of ambient wind flow around an isolated tree [J]. *Journal of Donghua University (English Edition)*, 2017, 34(2): 304-309.

[18] WANG Q F, LI M X, XU W B, et al. Review on liquid film flow and heat transfer characteristics outside horizontal tube falling film evaporator: CFD numerical simulation [J]. *International Journal of Heat and Mass Transfer*, 2020, 163: 120440.
[19] LI M Y, ZHAO X Z, YE Z T, et al. Study of wave-induced mass transport and internal mixing based on a two-liquid VOF model [J]. *Ocean Engineering*, 2019, 194: 106569.
[20] AKHLAGHI M, MOHAMMADI V, NOURI N M, et al. Multi-fluid VOF model assessment to simulate the horizontal air-water intermittent flow [J]. *Chemical Engineering Research and Design*, 2019, 152: 48-59.
[21] WU L, GONG M, WANG J T. Development of a DEM-VOF model for the turbulent free-surface flows with particles and its application to stirred mixing system [J]. *Industrial & Engineering Chemistry Research*, 2018, 57(5): 1714-1725.
[22] SHI J, GOURMA M, YEUNG H. CFD simulation of horizontal oil-water flow with matched density and medium viscosity ratio in different flow regimes [J]. *Journal of Petroleum Science and Engineering*, 2017, 151: 373-383.
[23] XIE R, WEI Y X, ZHANG Y G, et al. Flow model fitting and dynamic viscoelastic analysis of fenugreek gum solution [J]. *Journal of Food and Biotechnology*, 2018, 37: 4-49. (in Chinese)

薄膜蒸发器流场数值模拟及流态划分

陈 星, 彭倚天*, 黄 瑶, 邹 鲲
东华大学 机械工程学院, 上海 201620

摘 要: 薄膜蒸发器的流场形态复杂, 对内部的流场形态进行有效划分和定量分析以及探究内部的流场分布和物质混合特性对提升薄膜蒸发器效率意义重大。采用计算流体动力学 (computational fluid dynamics, CFD) 数值模拟, 得到薄膜蒸发器内高黏度流体流场分布规律。研究发现交错打断叶片可以极大促进物质混合传输, 并对蒸发器壁面高黏度物质成膜有显著影响。此外, 提出了一种基于径向体积分数统计的流场状态识别方法, 可以定量描述薄膜蒸发器的内部流场。该方法将薄膜蒸发器内的高黏度物质划分为液膜态、交换态和液团态三种流态的物质并做定量描述。结果表明, 交换态物质可以连接液膜与液团, 完成物质混合交换与液膜更新, 维持液膜持续高效蒸发。

关键词: 流态划分; 物质混合; 薄膜蒸发器; 数值模拟